Supplementary Information for:

HOMO Inversion as a Strategy for Improving the Light-Absorption Properties of Fe(II) Chromophores

Sriparna Mukherjee,[a] David E. Torres[b] and Elena Jakubikova[a,]*

[a] Department of Chemistry, North Carolina State University, Raleigh, NC 27695, USA.
[b] Wake STEM Early College High School, 715 Barbour Dr., Raleigh, NC 27603, USA.
Current address: North Carolina State University, Raleigh, NC 27695
[*] E-mail: ejakubi@ncsu.edu.

Table of Contents

Figure S1. Frontier KS orbitals of $[Fe(tpy)_2]^{2+}$ complexes substituted by carboxylic acid groups at the 4' (**1a**), 4,4'' (**3a**), and 5,5'' (**4a**) positions. 4

Figure S2. Top: HOMO and LUMO energies, bottom: HOMO-LUMO gaps (red), and average % of electron density (%ρ_{el}) on the linker group in doubly degenerate LUMO (blue) for **2a-f** series of complexes. 5

Figure S3. Top: HOMO and LUMO energies, bottom: HOMO-LUMO gaps (red), and average % of electron density (%ρ_{el}) on the linker group in doubly degenerate LUMO (blue) for **3a-e** series of complexes. 5

Figure S4. Top: HOMO and LUMO energies, bottom: HOMO-LUMO gaps (red), and average % of electron density (%ρ_{el}) on the linker group in doubly degenerate LUMO (blue) for **4a-e** series of complexes. 6

Figure S5. Degenerate LUMO orbitals for **1b-f** with carboxylic acid (A) on the center pyridines and donor groups on the side pyridines. Surfaces are constructed with 0.04 isovalue. 6

Figure S6. Average percent of electron density on a single donor group for the 21 lowest energy unoccupied orbitals near the frontier region for the **1c**, **1e**, and **1f**. Note that average density equal to 25% means that the MO is fully localized on the donor groups. 7

Figure S7. First singlet excitation of **1a-f** obtained from the TD-DFT that has contribution mostly from the HOMO to LUMO transition. 7

Figure S8. Lowest energy singlet excitations of **1a-f** obtained from TD-DFT. The shaded plots indicate transitions from HOMO into an e_g* orbital. 8

Figure S9. Left: the KS orbital diagram of pyridine, **5b** and **b**. Right: the KS orbital diagram of the pyridine, **5c** and **c**. Interactions between the orbitals are shown with dashed lines. LUMO orbitals are marked in green. 8

Figure S10. The KS orbital diagrams of **5c**, **6**, **5d** and **5e** derived from the interaction of pyridine with their respective donor groups. The relevant orbitals are highlighted. Interactions between the orbitals are shown with dashed lines. LUMO orbitals are marked in green. 9

Figure S11. The KS energy levels of pyridine and the donor groups (furan, thiophene, selenophene). The red lines are the orbitals that are interacting when the donor group is attached to the pyridine at its 4 position. 9

Figure S12. The effect of the change in the dihedral (marked in green) on the energy levels of **5b** (left) and **5c** (right). The red lines are the KS orbitals involved in interaction. 10

Figure S13. Left: the KS orbital energies of **5c** and **6**. Right: schematics of KS orbitals for the energy levels highlighted on the left in the order of increasing energy. 10

Figure S14. Electron density on Fe (ρ^{Fe}) of the 21 higher energy occupied orbitals near the frontier region for the **1a-d**. The KS orbitals with electron distribution ≥ 20 % are shown in red and among these the doubly degenerate orbitals are labeled as '*'. 11

Figure S15. Excited states for **1a**. Excited states were characterized for wavelengths > 350 nm with oscillator strength (f_{osc}) ≥ 0.01. Only those hole-particle pairs were considered whose contributions add up to ≥ 70 %. 11

Figure S16. Excited states for **1c**. Excited states were characterized for wavelengths > 350 nm with oscillator strength (f_{osc}) ≥ 0.01. Only those hole-particle pairs were considered whose contributions add up to ≥ 70 %. 13

Figure S17. Excited states for **1e**. Excited states were characterized for wavelengths > 350 nm with oscillator strength (f_{osc}) ≥ 0.01. Only those hole-particle pairs were considered whose contributions add up to ≥ 70 %. Transitions were classified as metal-centered (MC), metal-to-ligand charge transfer (MLCT), intra-ligand charge transfer (ILCT), intra-ligand charge transfer with some inter-ligand contribution (ILCT′), or ligand-centered (LC) based on visual inspection. 17

Figure S18. Excited states for **1f**. Excited states were characterized for wavelengths > 350 nm with oscillator strength (f_{osc}) ≥ 0.01. Only those hole-particle pairs were considered whose contributions add up to ≥ 70 %. Transitions were classified as metal-centered (MC), metal-to-ligand charge transfer (MLCT), intra-ligand charge transfer (ILCT), intra-ligand charge transfer with some inter-ligand contribution (ILCT′), or ligand-centered (LC) based on visual inspection. 22

Figure S19. Mixed transition examples for **1e**. Only the hole-particle pairs whose contributions add up to ≥ 70 % were considered in the assignment. Electron density on Fe (ρ^{Fe}) is given in parenthesis. Transitions were classified as metal-centered (MC), metal-to-ligand charge transfer (MLCT), intra-ligand charge transfer (ILCT), intra-ligand charge transfer with some inter-ligand contribution (ILCT′), or ligand-centered (LC) based on visual inspection. 23

Figure S20. Calculated UV-Vis spectra with TD-DFT employing CAM-B3LYP functional for **1a**, **1c**, **1e** and **1f**. 23

Figure S21. Calculated UV-Vis spectra of **1a**, **1e-L** and **1e**. **1e-L** denotes a ligand only structure obtained from the optimized geometry of **1e**. 24

Figure S22. Calculated UV-Vis spectra of **1a**, **1f-L** and **1f**. **1f-L** denotes a ligand only structure obtained from the optimized geometry of **1f**. 25

Figure S23. Electronic properties of **1c** series of complexes. Top: HOMO and LUMO energies. Bottom: HOMO-LUMO gaps (red) and average % of electron density on the carboxylic acid in doubly degenerate LUMO (blue). 25

Figure S24. Calculated UV-Vis spectra with TD-DFT employing CAM-B3LYP functional for **1a**, **1h**, **1c** and **1c′′′′**. 26

Figure S25. Excited states for 1h. Excited states were characterized for wavelengths > 350 nm with oscillator strength (f_{osc}) ≥ 0.01. Only those hole-particle pairs were considered whose contributions add up to ≥ 70 %. 26

Figure S26. Excited states for **1c′′′′**. Excited states were characterized for wavelengths > 350 nm with oscillator strength (f_{osc}) ≥ 0.01. Only those hole-particle pairs were considered whose contributions add up to ≥ 70 %. Transitions were classified as metal-centered (MC), metal-to-ligand charge transfer (MLCT), intra-ligand charge transfer (ILCT), intra-ligand charge transfer with some inter-ligand contribution (ILCT′), or ligand-centered (LC) based on visual inspection. 31

Figure S27. Calculated UV-Vis spectra employing TD-DFT for **1a**, **1h**, **1f** and **1f′**. Oscillator strength of the transitions are in the bottom plots. 32

Figure S28. Electron density on Fe (ρ^{Fe}) for the 21 highest energy occupied orbitals near the frontier region for **1a**, **1h**, **1f**, **1f′**. The KS orbitals with electron distribution ≥ 20% are shown in red and among these the doubly degenerate orbitals are labeled with *. 32

Figure S29. Calculated UV-Vis spectra, with CAM-B3LYP functional, of $[Fe(CNC)_2]^{2+}$ and complex with conjugated thiophene substituent on 4' position CNC. 33

Figure S30. Electron density on Fe (ρ^{Fe}) of the 21 higher energy occupied orbitals near the frontier region for $[Fe(CNC)_2]^{2+}$ and the complex with conjugated thiophene substituent on 4' position of CNC. The KS orbitals with electron distribution ≥ 20% are shown in red and among these the doubly degenerate orbitals are labeled as '*'. The red '*' indicates energy levels with difference in energy by 0.01 eV. 33

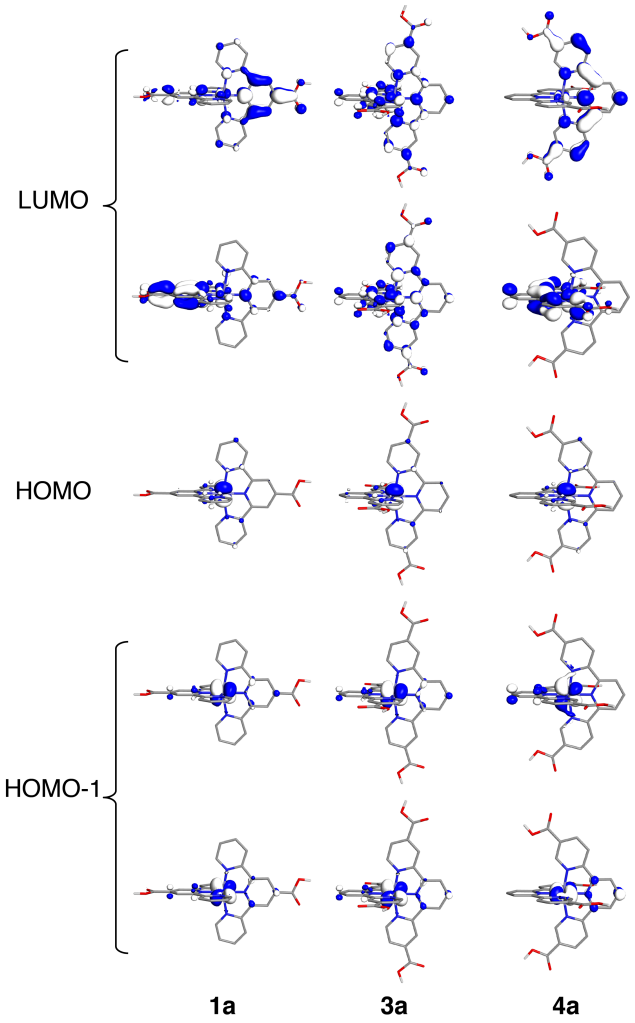

Figure S1. Frontier KS orbitals of $[Fe(tpy)_2]^{2+}$ complexes substituted by carboxylic acid groups at the 4' (**1a**), 4,4" (**3a**), and 5,5" (**4a**) positions.

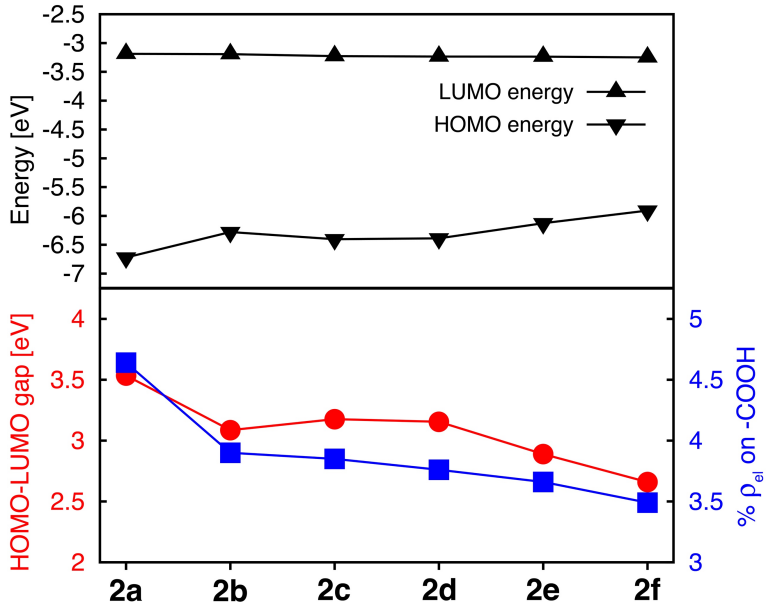

Figure S2. Top: HOMO and LUMO energies, bottom: HOMO-LUMO gaps (red), and average % of electron density (%ρ_{el}) on the linker group in doubly degenerate LUMO (blue) for **2a-f** series of complexes.

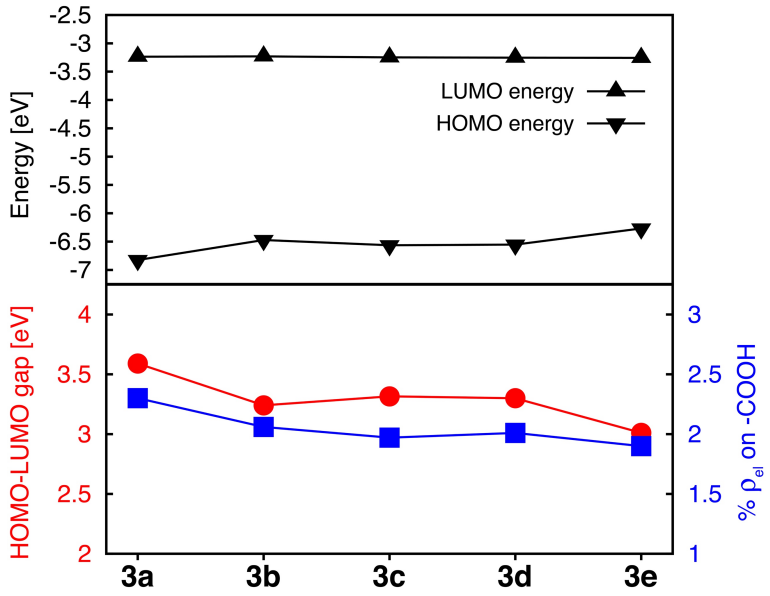

Figure S3. Top: HOMO and LUMO energies, bottom: HOMO-LUMO gaps (red), and average % of electron density (%ρ_{el}) on the linker group in doubly degenerate LUMO (blue) for **3a-e** series of complexes.

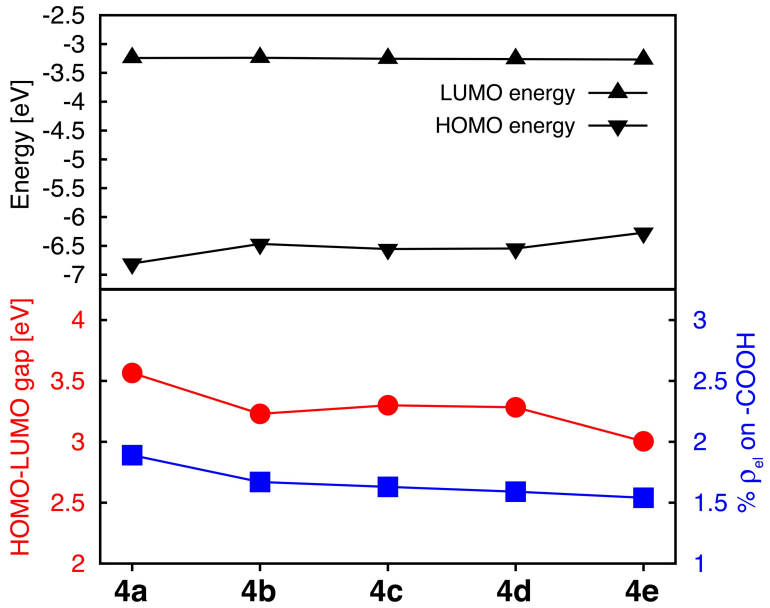

Figure S4. Top: HOMO and LUMO energies, bottom: HOMO-LUMO gaps (red), and average % of electron density (%ρ_{el}) on the linker group in doubly degenerate LUMO (blue) for **4a-e** series of complexes.

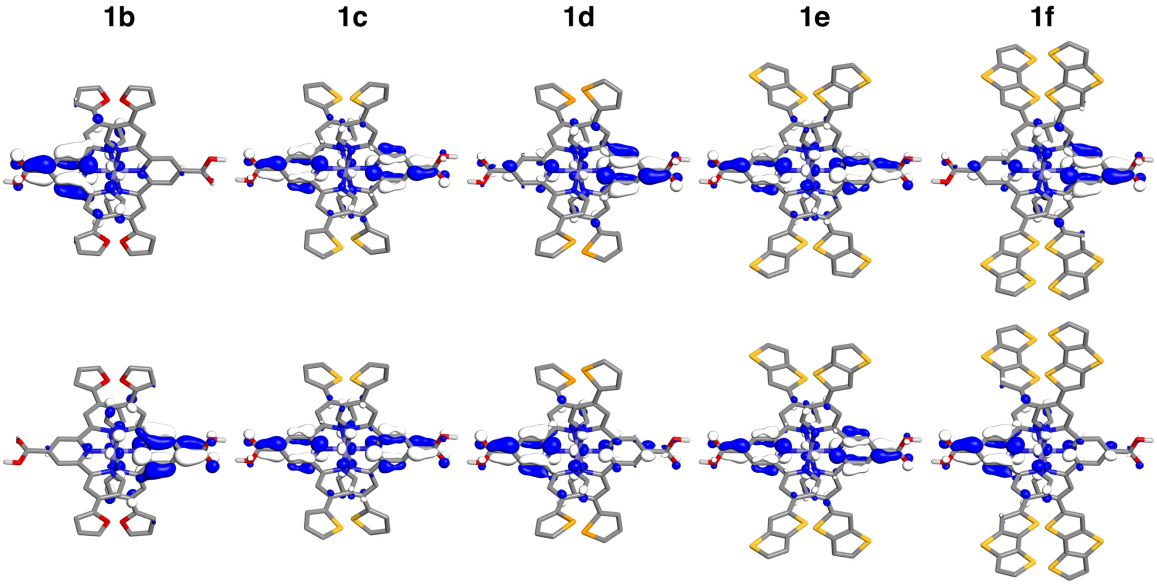

Figure S5. Degenerate LUMO orbitals for **1b-f** with carboxylic acid (A) on the center pyridines and donor groups on the side pyridines. Surfaces are constructed with 0.04 isovalue.

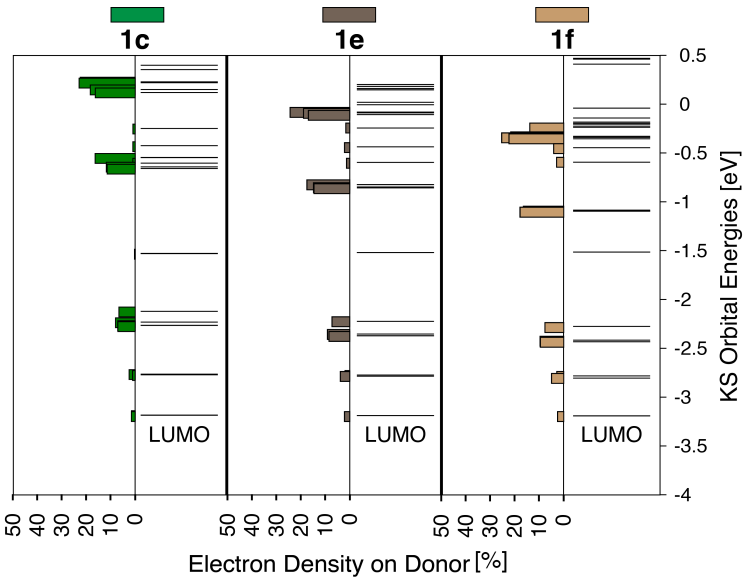

Figure S6. Average percent of electron density on a single donor group for the 21 lowest energy unoccupied orbitals near the frontier region for the **1c**, **1e**, and **1f**. Note that average density equal to 25% means that the MO is fully localized on the donor groups.

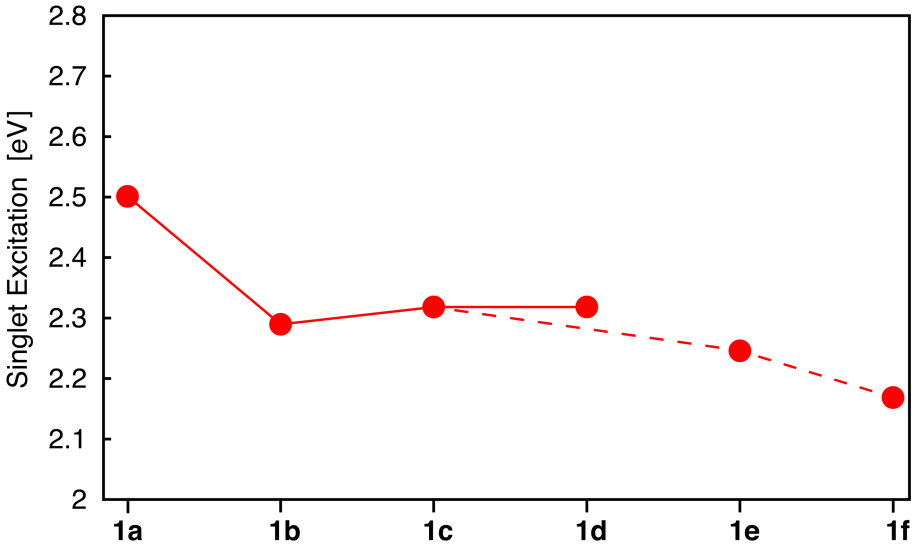

Figure S7. First singlet excitation of **1a-f** obtained from the TD-DFT that has contribution mostly from the HOMO to LUMO transition.

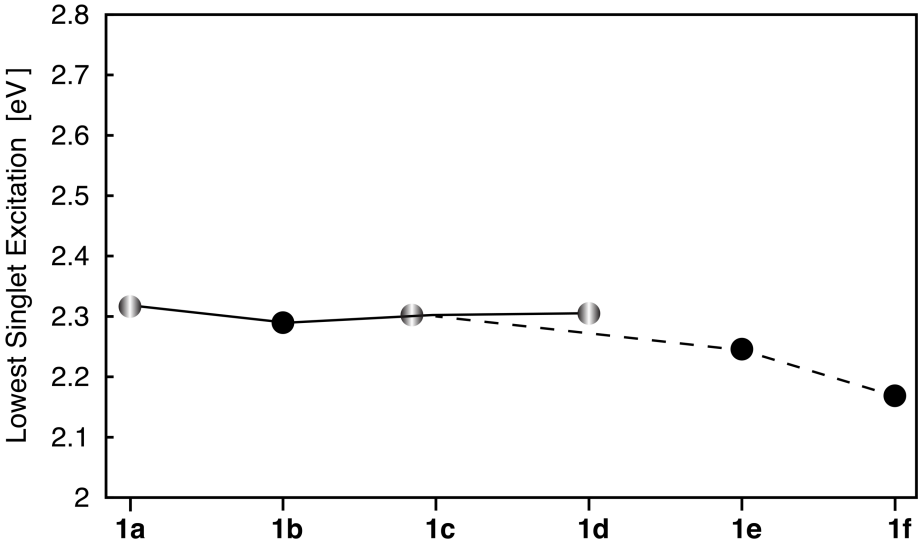

Figure S8. Lowest energy singlet excitations of **1a-f** obtained from TD-DFT. The shaded plots indicate transitions from HOMO into an e_g* orbital.

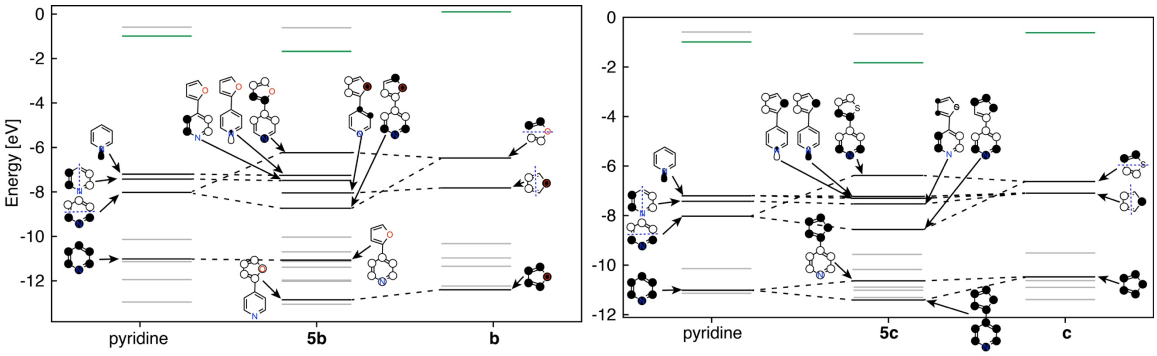

Figure S9. Left: the KS orbital diagram of pyridine, **5b** and **b**. Right: the KS orbital diagram of the pyridine, **5c** and **c**. Interactions between the orbitals are shown with dashed lines. LUMO orbitals are marked in green.

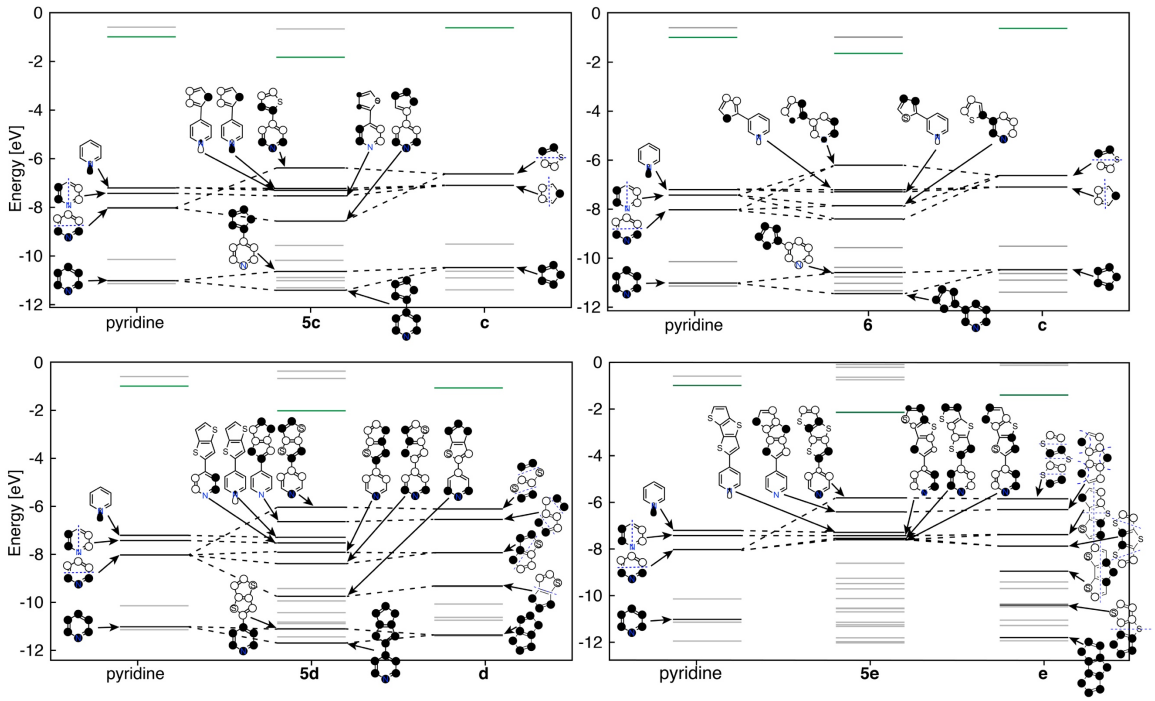

Figure S10. The KS orbital diagrams of **5c**, **6**, **5d** and **5e** derived from the interaction of pyridine with their respective donor groups. The relevant orbitals are highlighted. Interactions between the orbitals are shown with dashed lines. LUMO orbitals are marked in green.

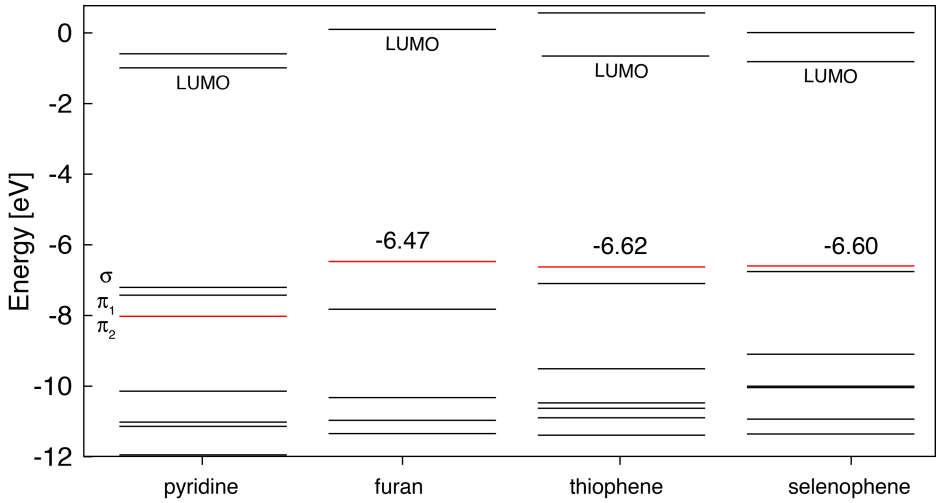

Figure S11. The KS energy levels of pyridine and the donor groups (furan, thiophene, selenophene). The red lines are the orbitals that are interacting when the donor group is attached to the pyridine at its 4 position.

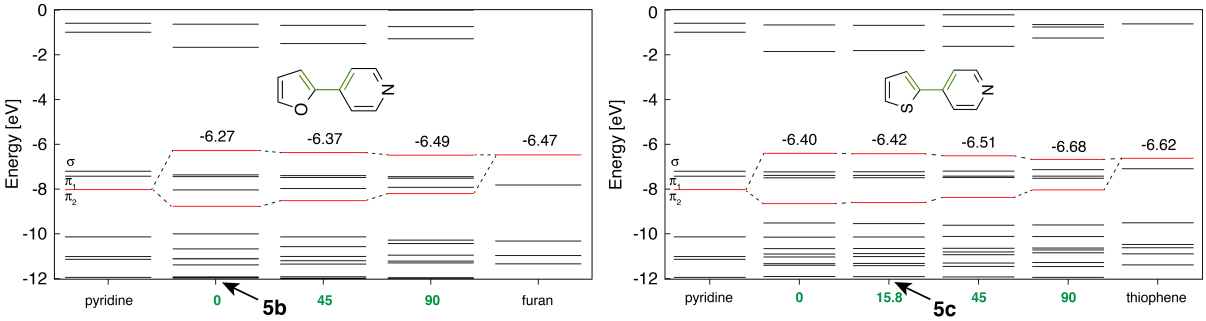

Figure S12. The effect of the change in the dihedral (marked in green) on the energy levels of **5b** (left) and **5c** (right). The red lines are the KS orbitals involved in interaction.

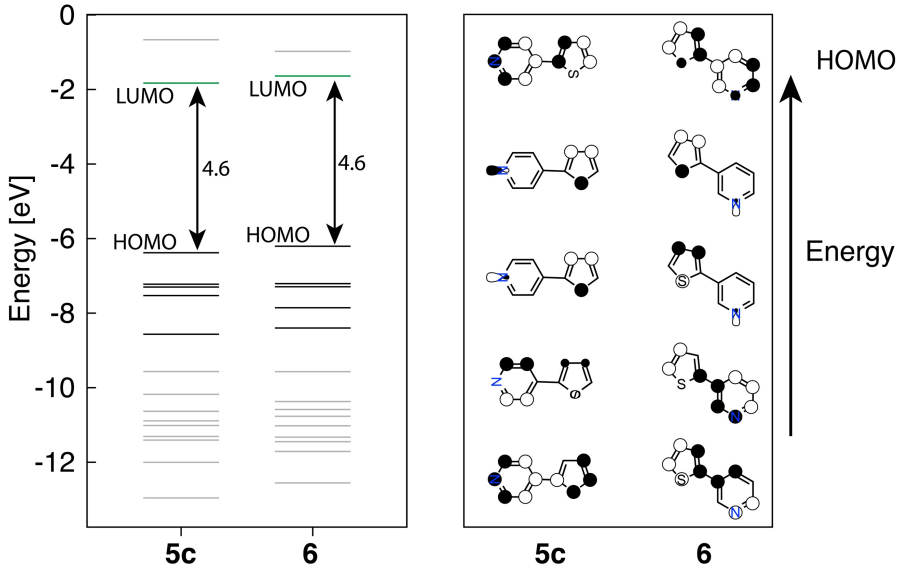

Figure S13. Left: the KS orbital energies of **5c** and **6**. Right: schematics of KS orbitals for the energy levels highlighted on the left in the order of increasing energy.

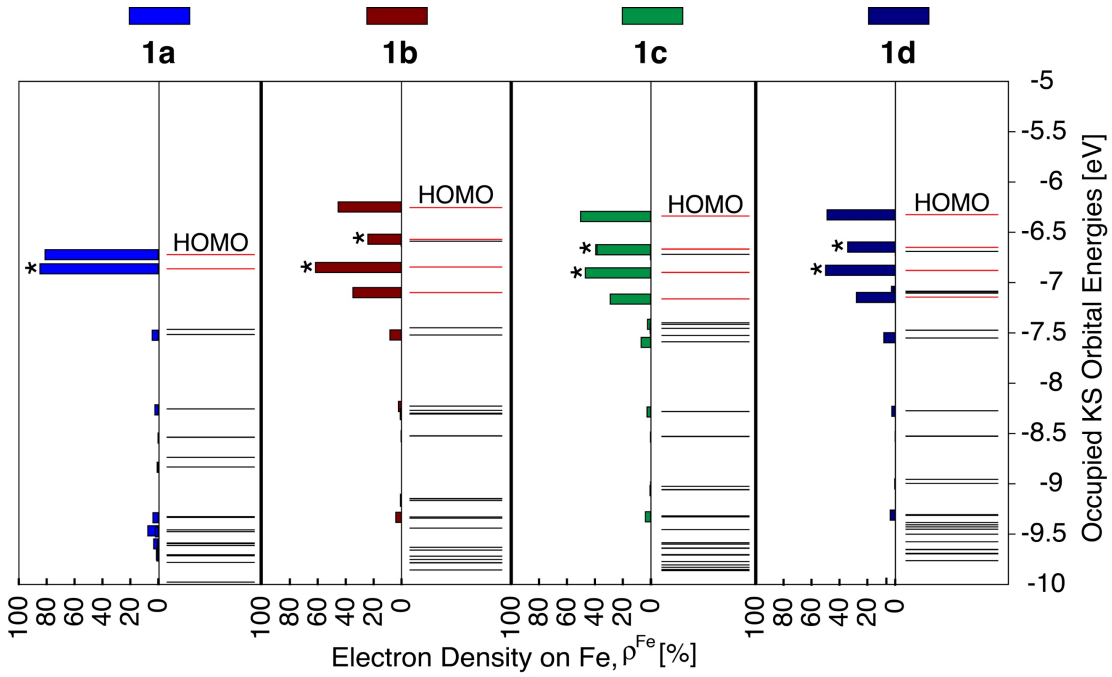

Figure S14. Electron density on Fe (ρ^{Fe}) of the 21 higher energy occupied orbitals near the frontier region for the **1a-d**. The KS orbitals with electron distribution ≥ 20 % are shown in red and among these the doubly degenerate orbitals are labeled as '*'.

Excited state	Hole state	Contribution	Particle state	Characteristic
λ = 442.03 nm f_{osc} = 0.1698	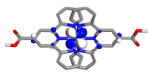 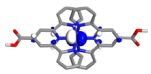	47.16% 47.16%	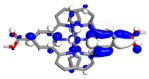 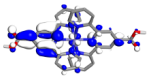	MLCT
λ = 389.65 nm f_{osc} = 0.0102	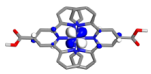	84.7%	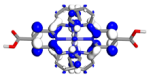	MLCT
λ = 389.65 nm f_{osc} = 0.0102	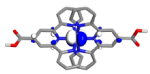	84.7%	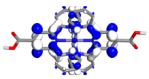	MLCT
λ = 386.67 nm f_{osc} = 0.0598	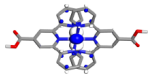	97.4%	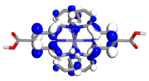	MLCT

Figure S15. Excited states for **1a**. Excited states were characterized for wavelengths > 350 nm with oscillator strength (f_{osc}) ≥ 0.01. Only those hole-particle pairs were considered whose contributions add up to ≥ 70 %.

Excited state	Hole state → Contribution → Particle state	Characteristic
λ = 534.84 nm f_{osc} = 0.0439	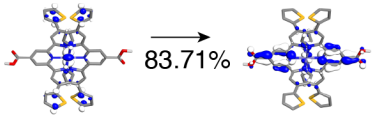	MLCT, ILCT
λ = 534.41 nm f_{osc} = 0.0421	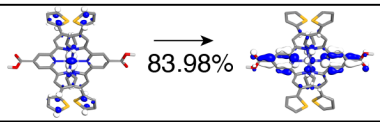	MLCT, ILCT
λ = 456.57 nm[a] f_{osc} = 0.0271	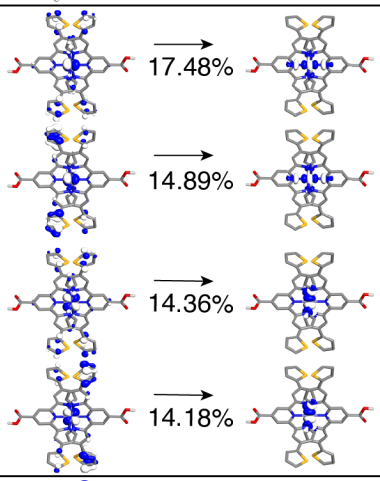	MC
λ = 456.32 nm f_{osc} = 0.1622	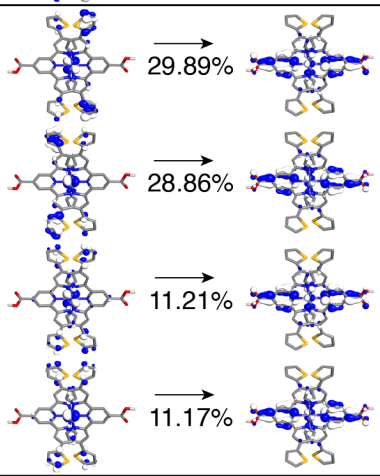	MLCT, ILCT
λ = 422.19 nm f_{osc} = 0.058	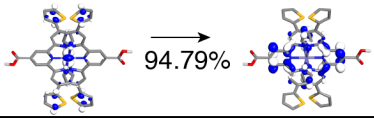	MLCT, ILCT
λ = 403.95 nm f_{osc} = 0.0568	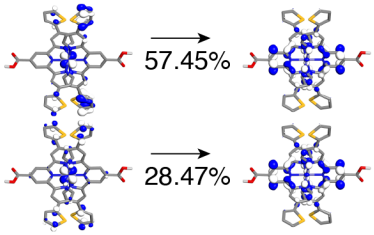	MLCT, ILCT

[a] Excitation with closely contributing hole-particle pairs hence only those with ≥ 10 % contribution were considered for characterization.

λ = 403.43 nm f_{osc} = 0.0572	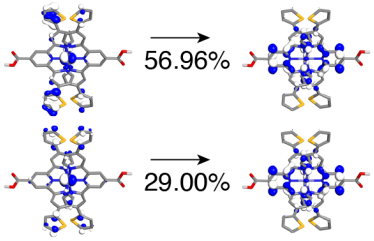	MLCT, ILCT
λ = 396.68 nm f_{osc} = 0.1158	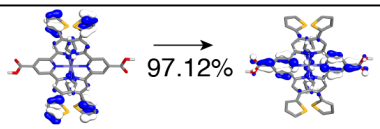	ILCT
λ = 396.42 nm f_{osc} = 0.1188	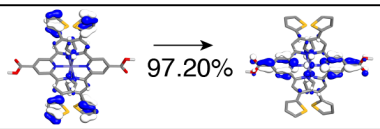	ILCT
λ = 386.60 nm f_{osc} = 0.0192	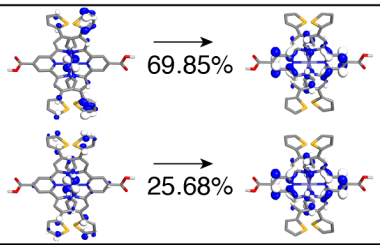	MLCT, ILCT
λ = 386.29 nm f_{osc} = 0.0183	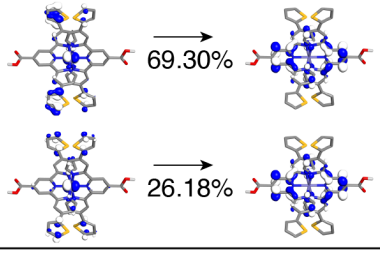	MLCT, ILCT
λ = 365.34 nm f_{osc} = 0.1791	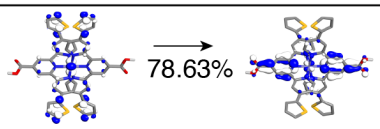	MLCT, ILCT
λ = 365.20 nm f_{osc} = 0.1700	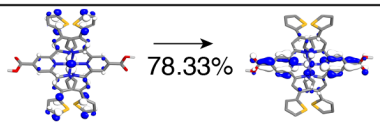	MLCT, ILCT
λ = 352.01 nm f_{osc} = 0.2934	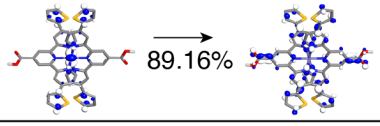	MLCT, ILCT
λ = 351.86 nm f_{osc} = 0.2866	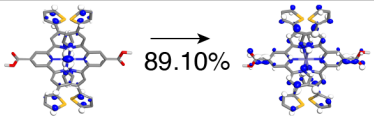	MLCT, ILCT

Figure S16. Excited states for **1c**. Excited states were characterized for wavelengths > 350 nm with oscillator strength (f_{osc}) ≥ 0.01. Only those hole-particle pairs were considered whose contributions add up to ≥ 70 %.

λ = 552.13 nm f_{osc} = 0.0973	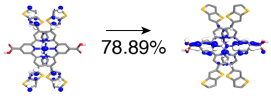	MLCT, ILCT
λ = 552.1 nm f_{osc} = 0.0972	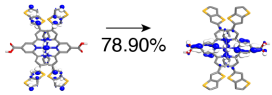	MLCT, ILCT
λ = 473.12 nm f_{osc} = 0.2283	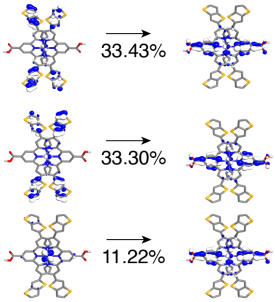	MLCT, ILCT
λ = 451.9 nm f_{osc} = 0.2086	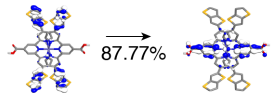	ILCT
λ = 451.89 nm f_{osc} = 0.2088	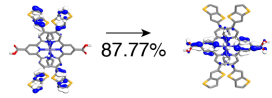	ILCT
λ = 440.67 nm f_{osc} = 0.0394		MLCT, ILCT
λ = 427.1 nm f_{osc} = 0.0397	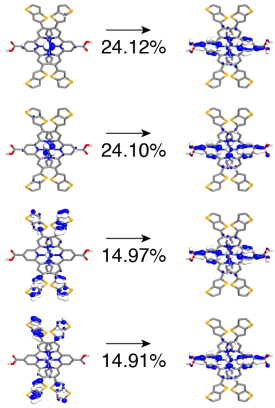	MLCT, ILCT
λ = 413.14 nm f_{osc} = 0.0924	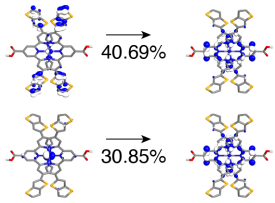	MLCT, ILCT
λ = 413.12 nm f_{osc} = 0.0922	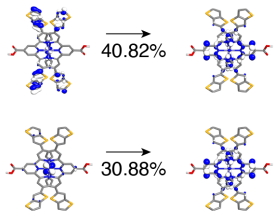	MLCT, ILCT

λ = 411.08 nm f_{osc} = 0.2075	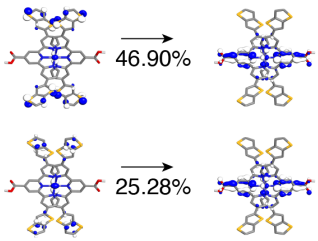	MLCT, ILCT
λ = 411.07 nm f_{osc} = 0.2074	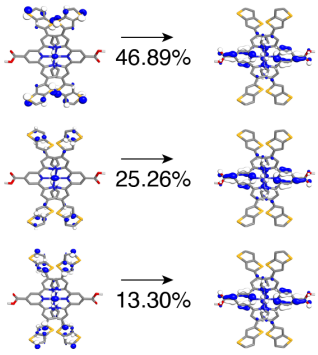	MLCT, ILCT
λ = 399.84 nm f_{osc} = 0.0352	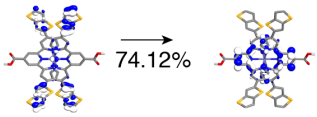	MLCT, ILCT
λ = 399.83 nm f_{osc} = 0.0353	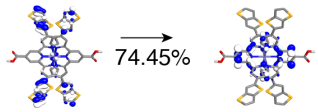	MLCT, ILCT
λ = 393.11 nm f_{osc} = 0.0253	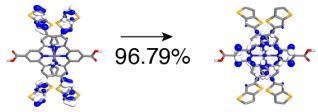	ILCT
λ = 383.35 nm f_{osc} = 0.0288	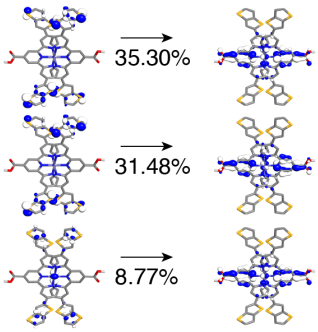	ILCT
λ = 383.35 nm f_{osc} = 0.029	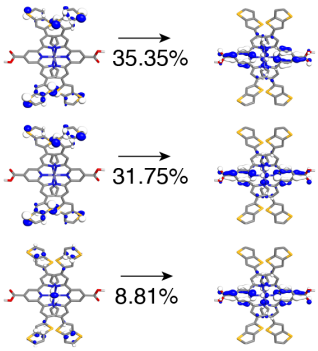	ILCT

λ = 379.61 nm[a] f_{osc} = 0.1974	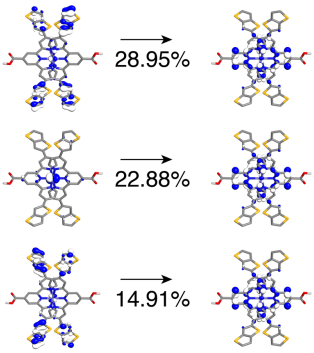	MLCT, ILCT
λ = 379.60 nm[a] f_{osc} = 0.1986	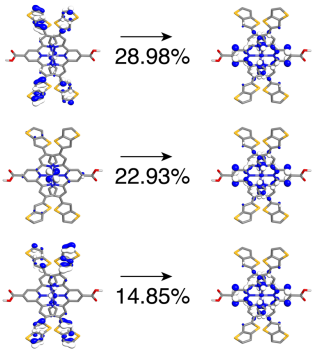	MLCT, ILCT
λ = 376.26 nm f_{osc} = 0.4392	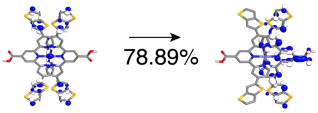	MLCT, ILCT′
λ = 376.24 nm f_{osc} = 0.4424	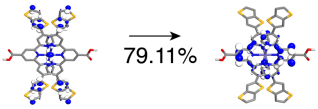	MLCT, ILCT
λ = 375.62 nm f_{osc} = 0.1001	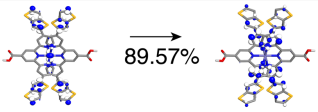	MLCT, ILCT
λ = 350.48 nm[a] f_{osc} = 0.787	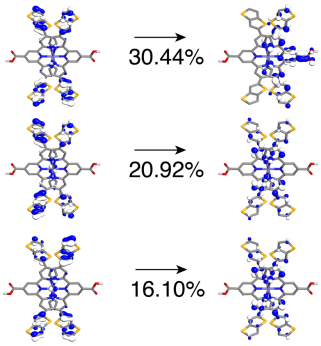	MLCT, ILCT′, LC

[a] Excitation with closely contributing hole-particle pairs hence only those with ≥ 10 % contribution were considered for characterization.

λ = 350.47 nm[a] f_{osc} = 0.7866	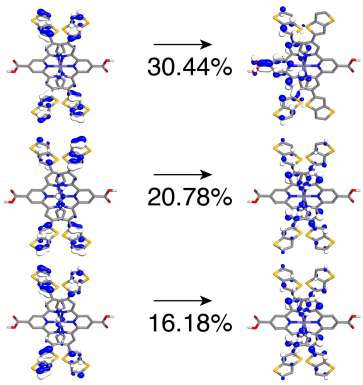	MLCT, ILCT′, LC

[a] Excitation with closely contributing hole-particle pairs hence only those with ≥ 10 % contribution were considered for characterization.

Figure S17. Excited states for **1e**. Excited states were characterized for wavelengths > 350 nm with oscillator strength (f_{osc}) ≥ 0.01. Only those hole-particle pairs were considered whose contributions add up to ≥ 70 %. Transitions were classified as metal-centered (MC), metal-to-ligand charge transfer (MLCT), intra-ligand charge transfer (ILCT), intra-ligand charge transfer with some inter-ligand contribution (ILCT′), or ligand-centered (LC) based on visual inspection.

λ = 571.76 nm f_{osc} = 0.1750	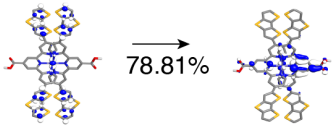	MLCT, ILCT
λ = 571.74 nm f_{osc} = 0.1748	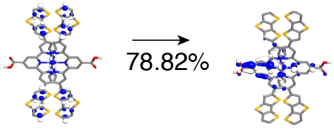	MLCT, ILCT
λ = 504.34 nm f_{osc} = 0.1217	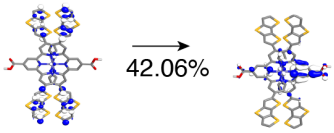 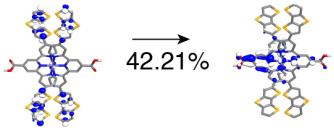	ILCT
λ = 495.08 nm f_{osc} = 0.2730	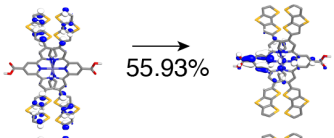 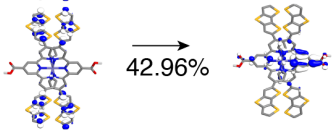	ILCT
λ = 495.08 nm f_{osc} = 0.2732	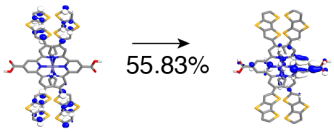 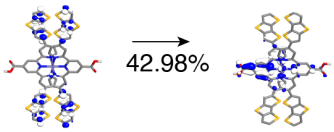	ILCT

λ = 460.00 nm f_{osc} = 0.0213	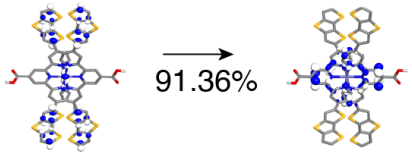	MLCT, ILCT
λ = 442.65 nm f_{osc} = 0.13687	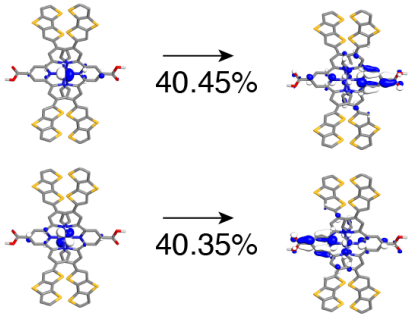	MLCT
λ = 436.44 nm f_{osc} = 0.3700	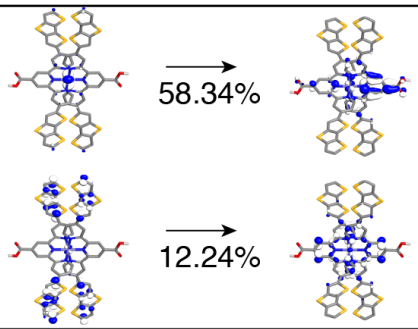	MLCT, ILCT
λ = 436.44 nm f_{osc} = 0.3702	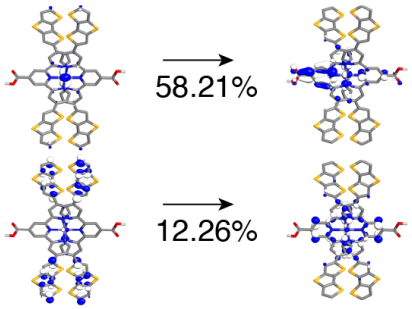	MLCT, ILCT
λ = 432.37 nm f_{osc} = 0.2186	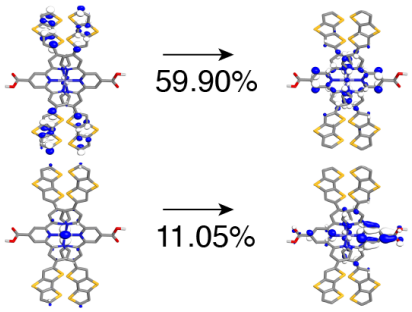	MLCT, ILCT

λ = 432.37 nm f_{osc} = 0.2179	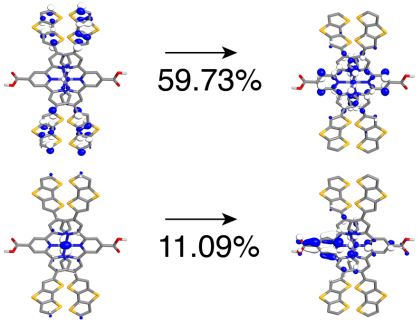	MLCT, ILCT
λ = 424.95 nm f_{osc} = 0.0102	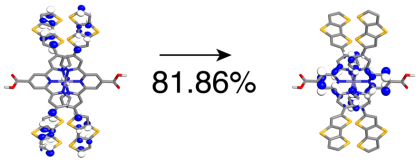	ILCT
λ = 400.08 nm f_{osc} = 0.8977	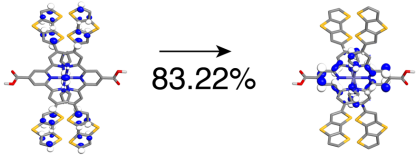	MLCT, ILCT
λ = 400.07 nm f_{osc} = 0.9039	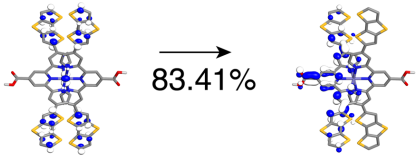	MLCT, ILCT′, LC
λ = 399.65 nm f_{osc} = 0.0484	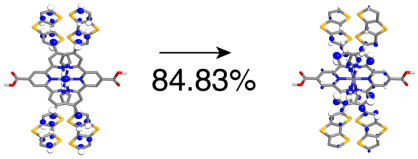	MLCT, ILCT, LC
λ = 380.95 nm f_{osc} = 0.2250	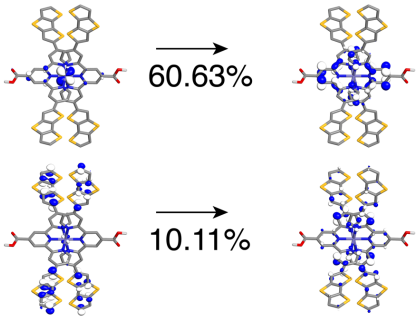	MLCT, ILCT, LC
λ = 380.94 nm f_{osc} = 0.2272	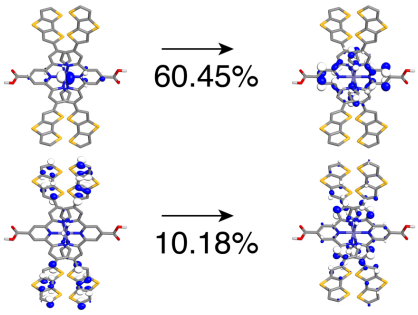	MLCT, ILCT, LC

λ = 378.75 nm f_{osc} = 0.3902	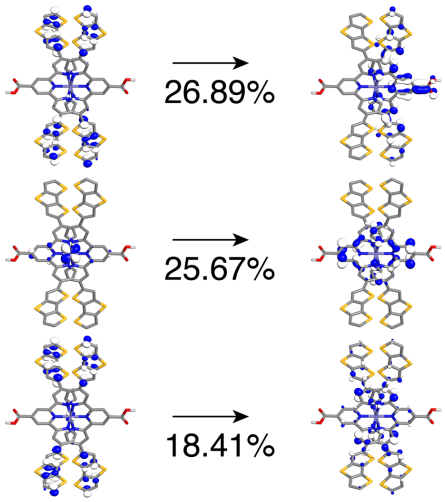	MLCT, ILCT′, LC
λ = 378.75 nm f_{osc} = 0.3888	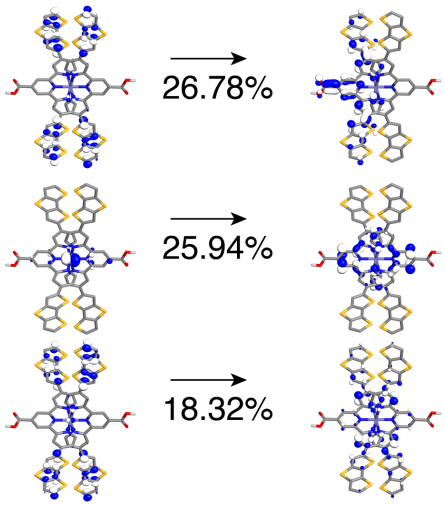	MLCT, ILCT, LC
λ = 376.40 nm f_{osc} = 0.0110	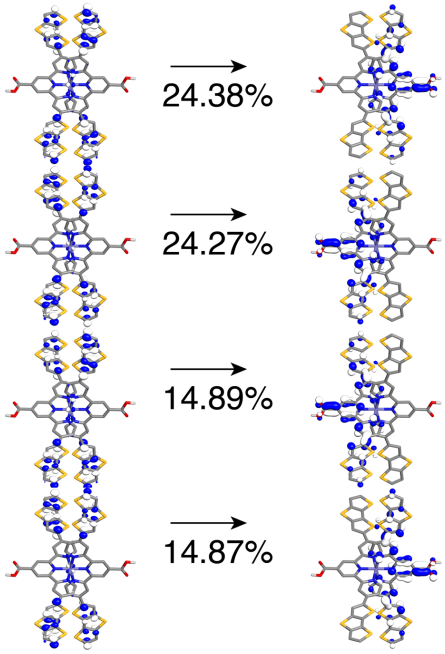	ILCT′, LC

λ = 365.66 nm f_{osc} = 0.0188	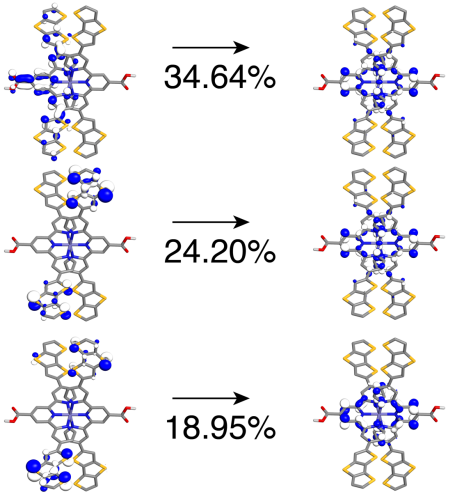	ILCT′, LC
λ = 365.35 nm f_{osc} = 0.0489	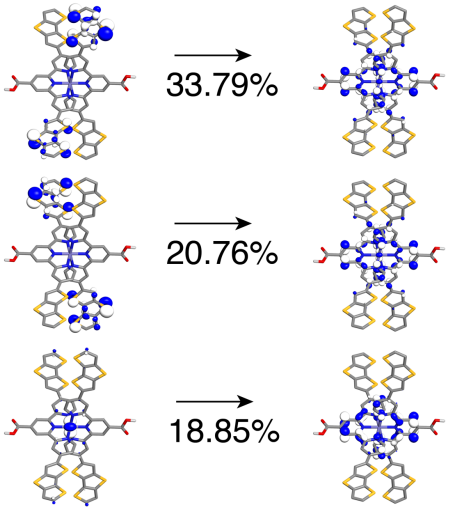	MLCT, ILCT
λ = 359.95 nm f_{osc} = 0.0888	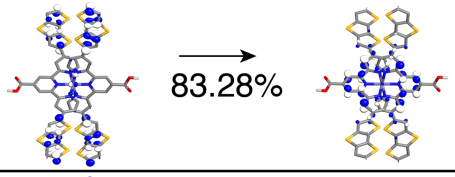	ILCT
λ = 359.93 nm f_{osc} = 0.0915	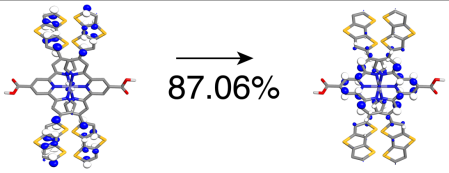	ILCT

Figure S18. Excited states for **1f**. Excited states were characterized for wavelengths > 350 nm with oscillator strength (f_{osc}) ≥ 0.01. Only those hole-particle pairs were considered whose contributions add up to ≥ 70 %. Transitions were classified as metal-centered (MC), metal-to-ligand charge transfer (MLCT), intra-ligand charge transfer (ILCT), intra-ligand charge transfer with some inter-ligand contribution (ILCT′), or ligand-centered (LC) based on visual inspection.

Excited state	Hole state → Particle state Contribution	Characteristic
λ = 376.26 nm f_{osc} = 0.4392	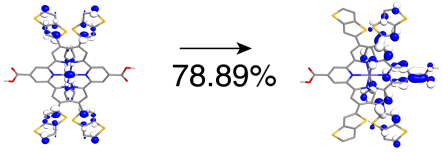	MLCT, ILCT′
λ = 413.12 nm f_{osc} = 0.0922	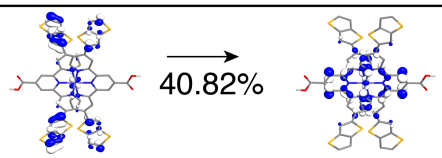 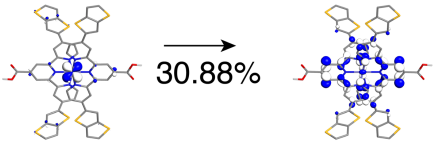	MLCT, ILCT

Figure S19. Mixed transition examples for **1e**. Only the hole-particle pairs whose contributions add up to ≥ 70 % were considered in the assignment. Electron density on Fe (ρ^{Fe}) is given in parenthesis. Transitions were classified as metal-centered (MC), metal-to-ligand charge transfer (MLCT), intra-ligand charge transfer (ILCT), intra-ligand charge transfer with some inter-ligand contribution (ILCT′), or ligand-centered (LC) based on visual inspection.

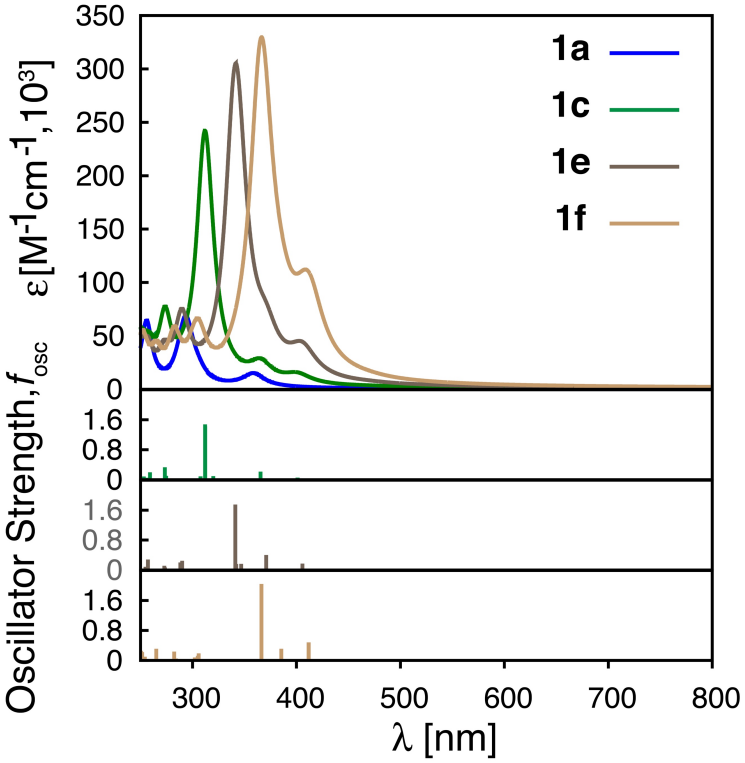

Figure S20. Calculated UV-Vis spectra with TD-DFT employing CAM-B3LYP functional for **1a, 1c, 1e** and **1f**.

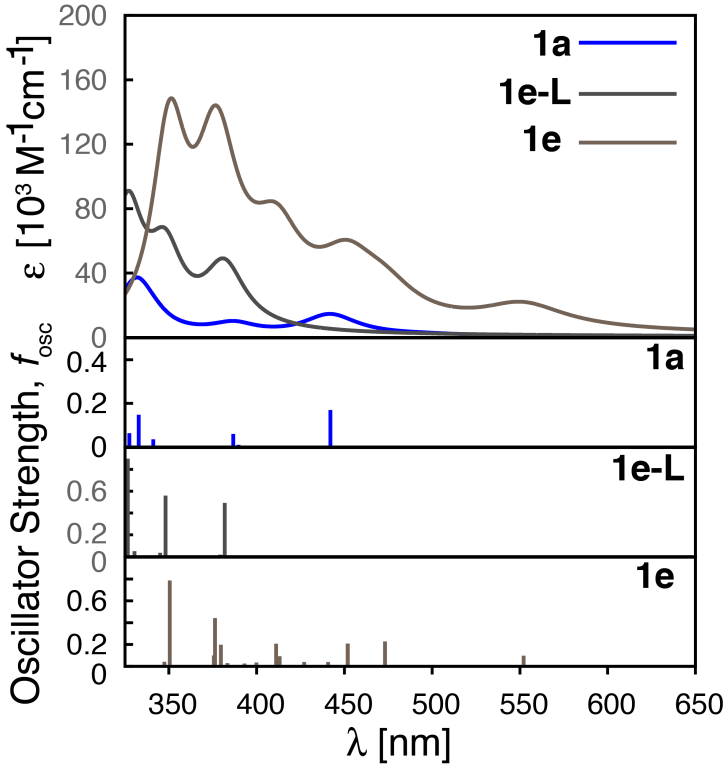

Figure S21. Calculated UV-Vis spectra of **1a**, **1e-L** and **1e**. **1e-L** denotes a ligand only structure obtained from the optimized geometry of **1e**.

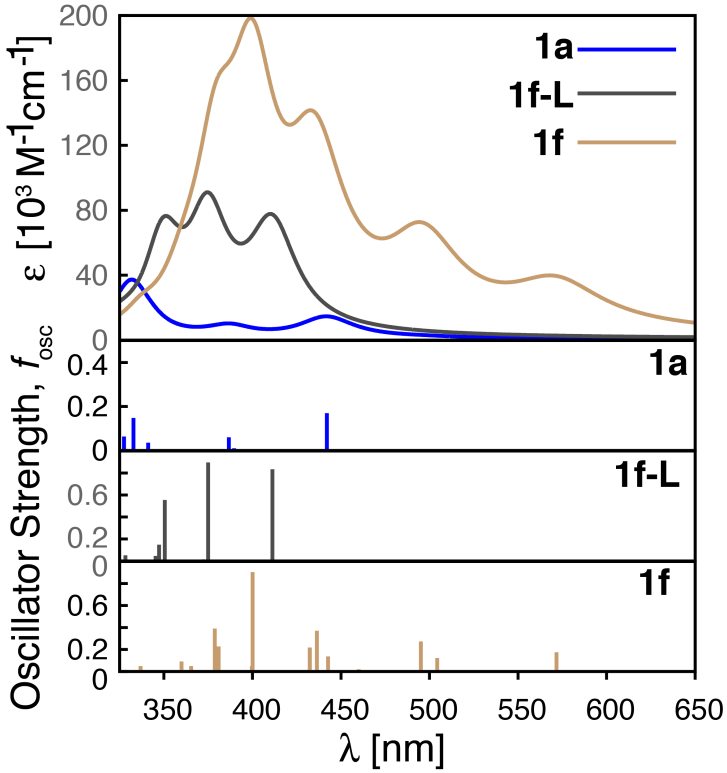

Figure S22. Calculated UV-Vis spectra of **1a**, **1f-L** and **1f**. **1f-L** denotes a ligand only structure obtained from the optimized geometry of **1f**.

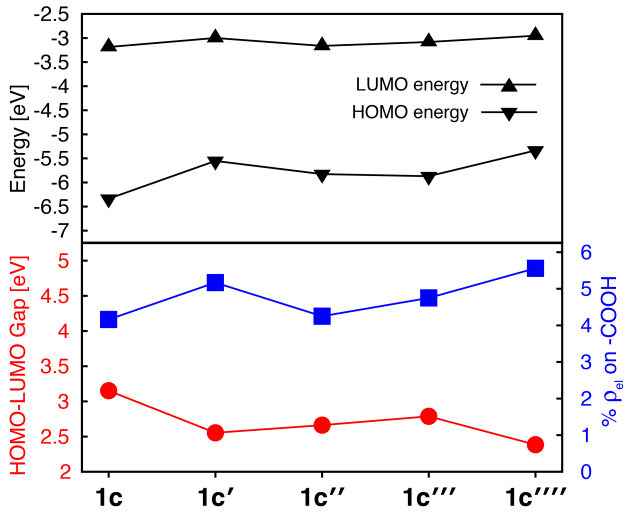

Figure S23. Electronic properties of **1c** series of complexes. Top: HOMO and LUMO energies. Bottom: HOMO-LUMO gaps (red) and average % of electron density on the carboxylic acid in doubly degenerate LUMO (blue).

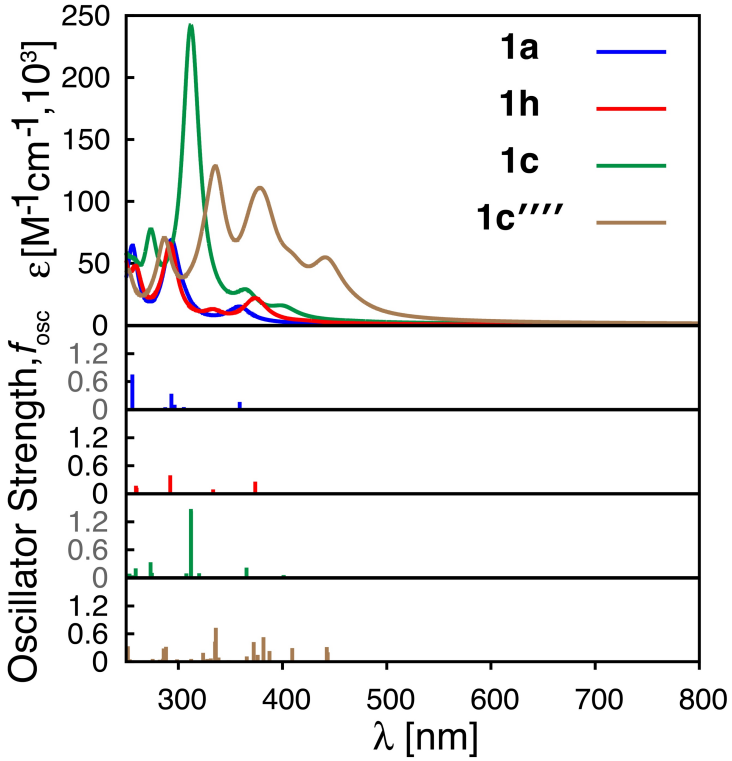

Figure S24. Calculated UV-Vis spectra with TD-DFT employing CAM-B3LYP functional for **1a, 1h, 1c** and **1c''''**.

Excited state	Hole state	Contribution	Particle state	Characteristic
λ = 468.82 nm f_{osc} = 0.1699	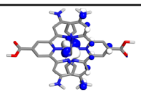 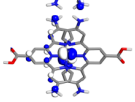	40.0% 39.9%	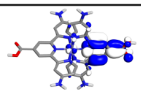 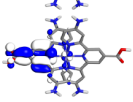	MLCT
λ = 448.83 nm f_{osc} = 0.1328	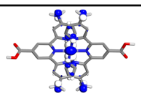	85.8%	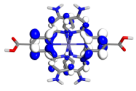	MLCT
λ = 401.62 nm f_{osc} = 0.0124	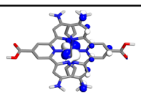	73.4%	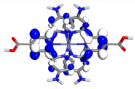	MLCT
λ = 401.60 nm f_{osc} = 0.0123	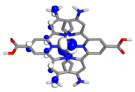	73.6%	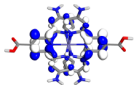	MLCT
λ = 380.36 nm f_{osc} = 0.0128	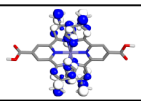	98.9%	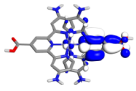	LC
λ = 380.34 nm f_{osc} = 0.0129	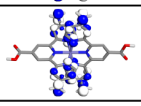	98.9%	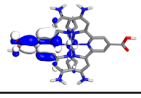	LC

Figure S25. Excited states for **1h**. Excited states were characterized for wavelengths > 350 nm with oscillator strength (f_{osc}) ≥ 0.01. Only those hole-particle pairs were considered whose contributions add up to ≥ 70 %.

λ = 671.96 nm f_{osc} = 0.056	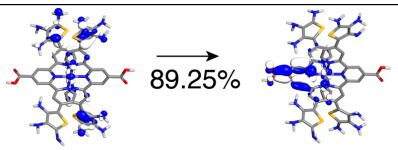	MLCT, ILCT′
λ = 660.9 nm f_{osc} = 0.1065	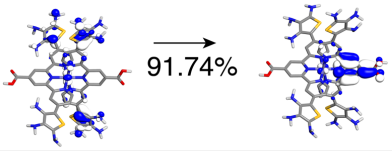	MLCT, ILCT′
λ = 598.63 nm f_{osc} = 0.0735	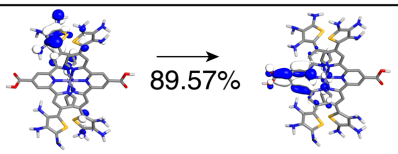	ILCT
λ = 588.69 nm f_{osc} = 0.0593	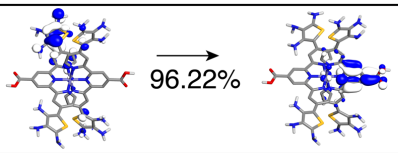	ILCT′
λ = 583.73 nm f_{osc} = 0.0318	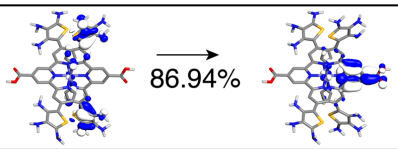	ILCT
λ = 541.61 nm f_{osc} = 0.0708	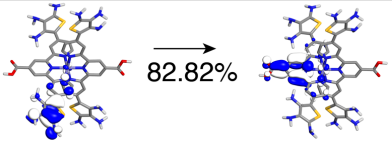	ILCT
λ = 534.13 nm f_{osc} = 0.0168	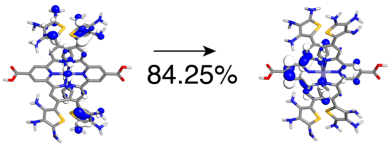	MLCT, ILCT
λ = 533.78 nm f_{osc} = 0.016	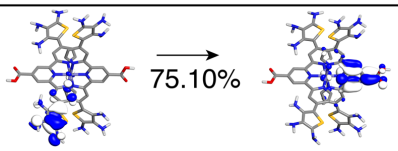	ILCT′
λ = 502.91 nm f_{osc} = 0.0184	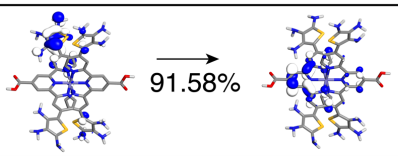	ILCT
λ = 497.89 nm f_{osc} = 0.0301	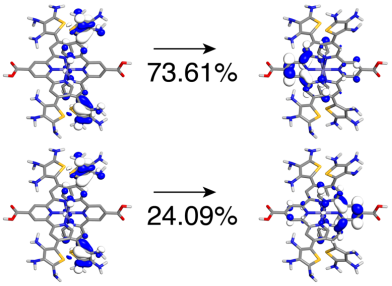	ILCT′
λ = 486.95 nm f_{osc} = 0.0239	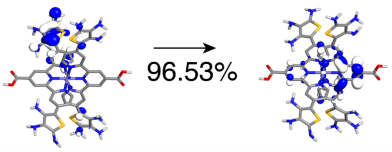	ILCT

λ = 486.05 nm f_{osc} = 0.0546	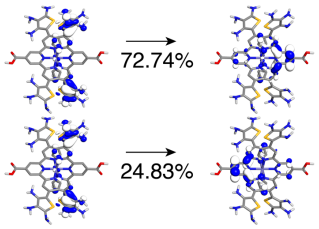	ILCT′
λ = 462.81 nm[a] f_{osc} = 0.0567	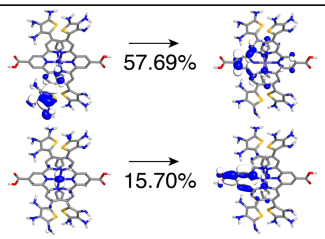	MLCT, ILCT
λ = 453.65 nm f_{osc} = 0.1654	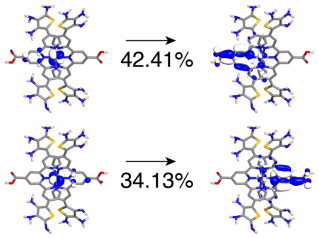	MLCT
λ = 449.24 nm[a] f_{osc} = 0.0329	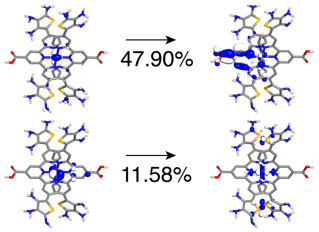	MLCT, MC
λ = 444.95 nm f_{osc} = 0.0292	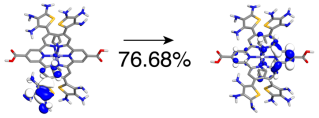	ILCT′
λ = 443.84 nm[a] f_{osc} = 0.0121	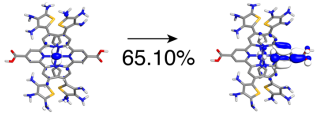	MLCT
λ = 406.15 nm f_{osc} = 0.014	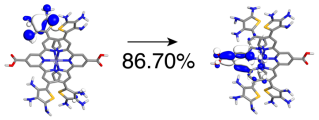	ILCT
λ = 405.38 nm f_{osc} = 0.0448	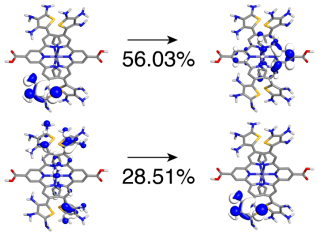	MLCT, ILCT′

[a] Excitation with closely contributing hole-particle pairs hence only those with ≥ 10 % contribution were considered for characterization.

λ = 404.22 nm f_{osc} = 0.0645	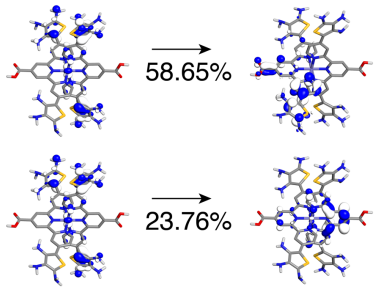	MLCT, ILCT′
λ = 396.86 nm f_{osc} = 0.0645	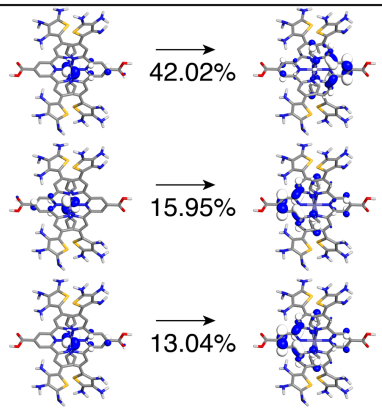	MLCT
λ = 396.26 nm f_{osc} = 0.0614	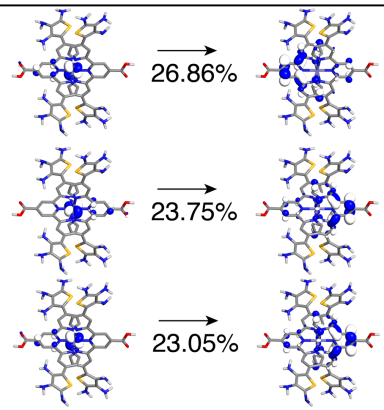	MLCT
λ = 392.13 nm f_{osc} = 0.7069	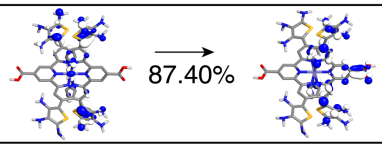	MLCT, ILCT
λ = 387.8 nm f_{osc} = 0.0275	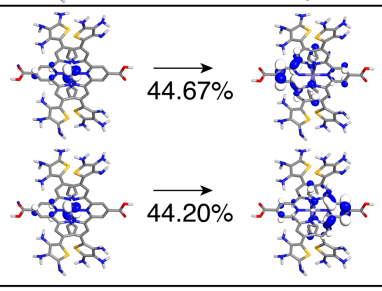	MLCT

λ = 386.04 nm f_{osc} = 0.2453	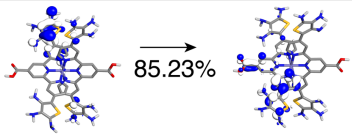	ILCT
λ = 383.41 nm[a] f_{osc} = 0.0896	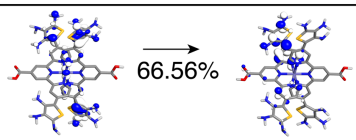	MLCT, ILCT
λ = 375.88 nm[a] f_{osc} = 0.0363	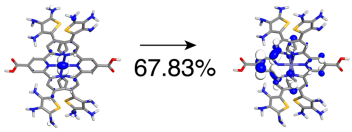	MLCT
λ = 374.94 nm f_{osc} = 0.3069	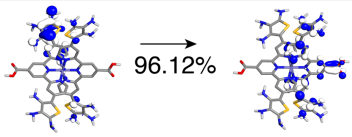	ILCT′
λ = 371.65 nm[a] f_{osc} = 0.2352	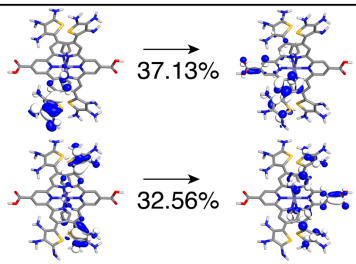	ILCT
λ = 369.19 nm[a] f_{osc} = 0.579	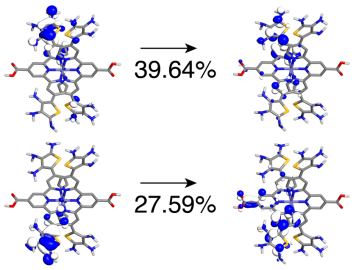	ILCT
λ = 368.73 nm f_{osc} = 0.0211	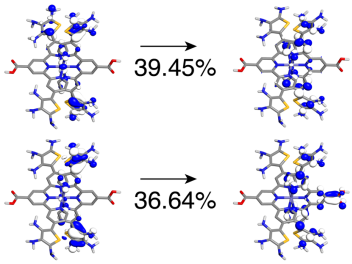	ILCT′
λ = 363.37 nm f_{osc} = 0.1948	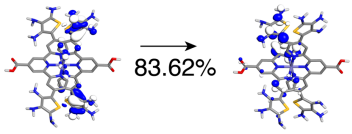	ILCT′

[a] Excitation with closely contributing hole-particle pairs hence only those with ≥ 10 % contribution were considered for characterization.

λ = 363.22 nm f_{osc} = 0.0414	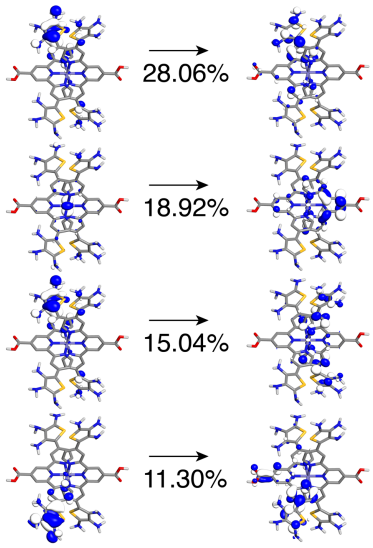	MLCT, ILCT′
λ = 361.36 nm f_{osc} = 0.2733	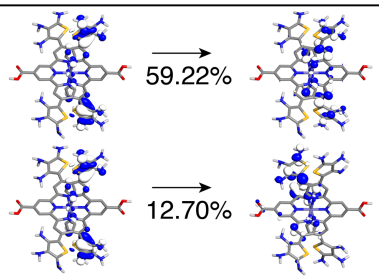	MLCT, ILCT′
λ = 355.89 nm f_{osc} = 0.0287	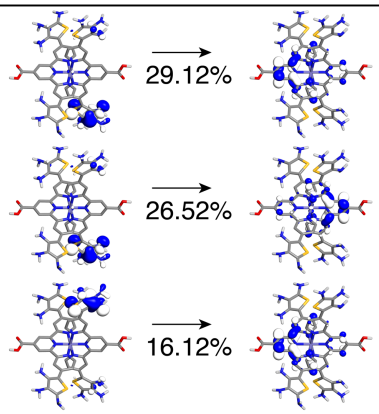	ILCT′
λ = 354.18 nm f_{osc} = 0.0599	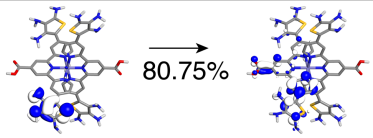	MLCT, ILCT

Figure S26. Excited states for **1c′′′′**. Excited states were characterized for wavelengths > 350 nm with oscillator strength (f_{osc}) ≥ 0.01. Only those hole-particle pairs were considered whose contributions add up to ≥ 70 %. Transitions were classified as metal-centered (MC), metal-to-ligand charge transfer (MLCT), intra-ligand charge transfer (ILCT), intra-ligand charge transfer with some inter-ligand contribution (ILCT′), or ligand-centered (LC) based on visual inspection.

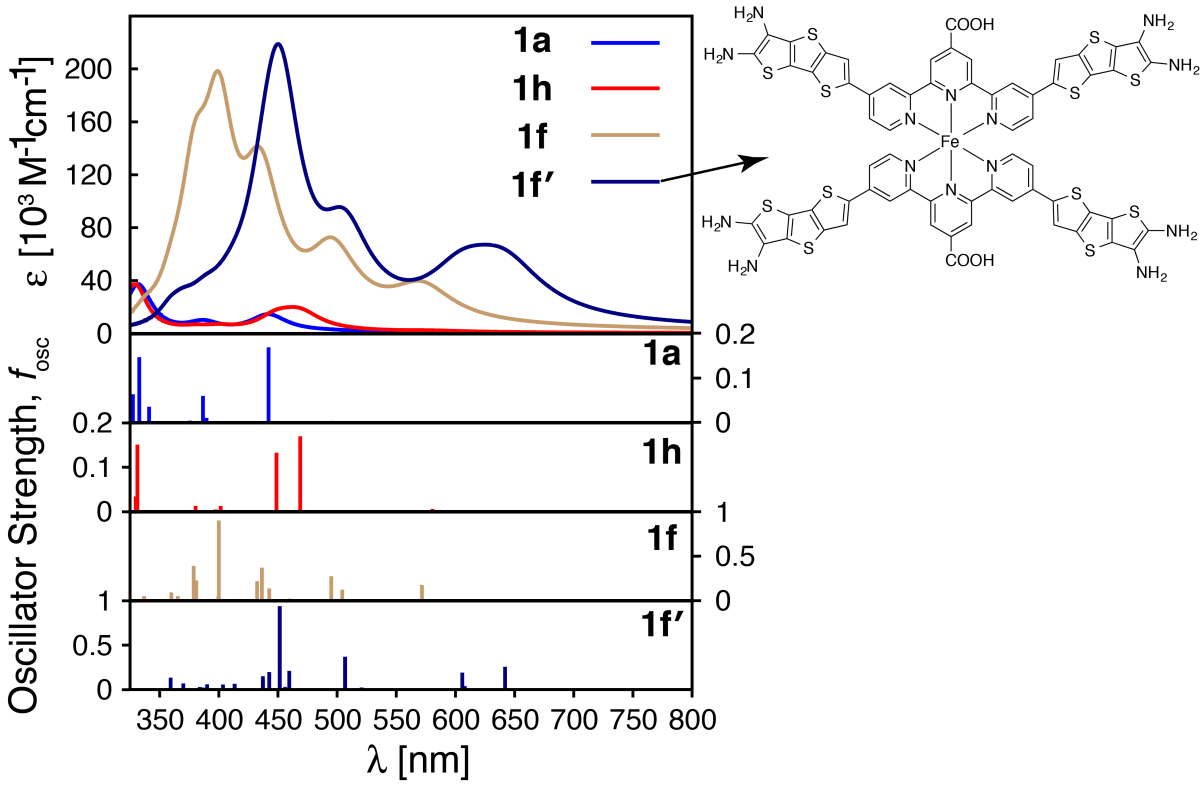

Figure S27. Calculated UV-Vis spectra employing TD-DFT for **1a**, **1h**, **1f** and **1f′**. Oscillator strength of the transitions are in the bottom plots.

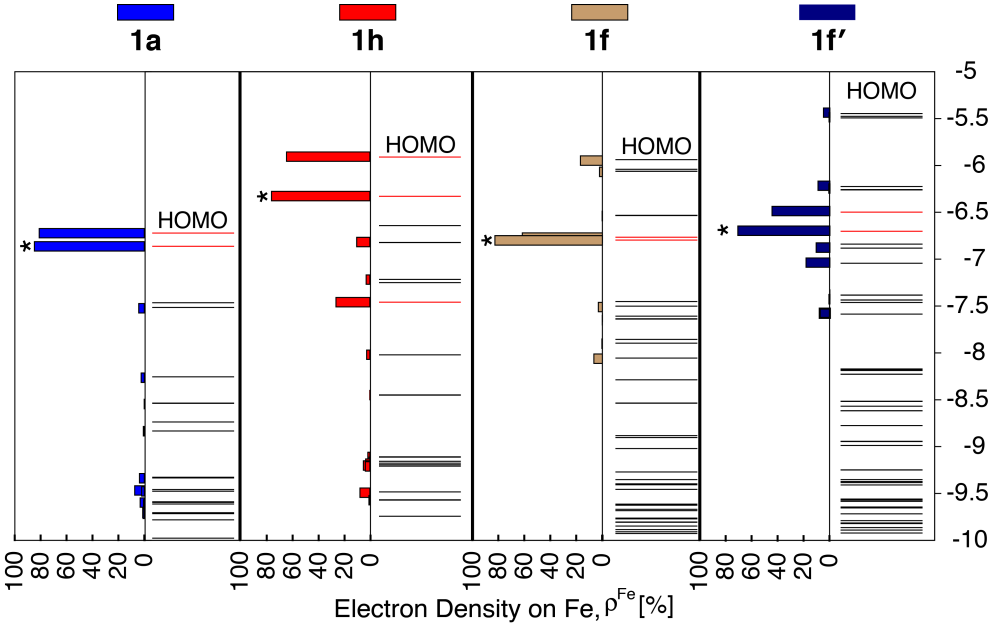

Figure S28. Electron density on Fe (ρ^{Fe}) for the 21 highest energy occupied orbitals near the frontier region for **1a**, **1h**, **1f**, **1f′** . The KS orbitals with electron distribution ≥ 20% are shown in red and among these the doubly degenerate orbitals are labeled with *.

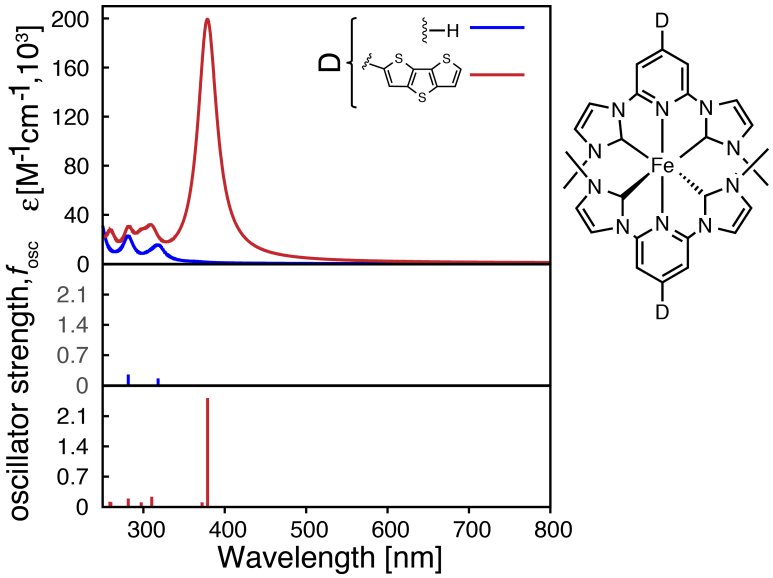

Figure S29. Calculated UV-Vis spectra, with CAM-B3LYP functional, of $[Fe(CNC)_2]^{2+}$ and complex with conjugated thiophene substituent on 4' position CNC.

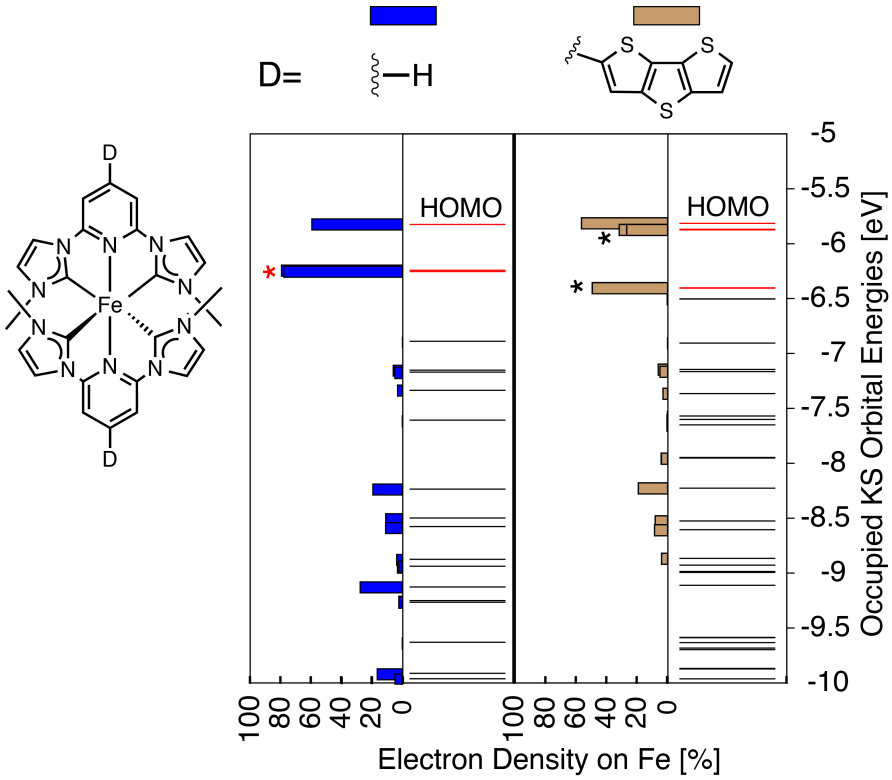

Figure S30. Electron density on Fe (ρ^{Fe}) of the 21 higher energy occupied orbitals near the frontier region for $[Fe(CNC)_2]^{2+}$ and the complex with conjugated thiophene substituent on 4' position of CNC. The KS orbitals with electron distribution ≥ 20% are shown in red and among these the doubly degenerate orbitals are labeled as '*'. The red '*' indicates energy levels with difference in energy by 0.01 eV.